Supporting Information

Solution- and solid-state photophysical and stimuli-responsive behavior in conjugated monoalkoxynaphthalene-naphthalimide donor-acceptor dyads.

Cameron Peebles, Christopher D. Wight, and Brent L. Iverson

Table of Contents……1

More details about the solution- and solid-state photophysical properties of **4**……2

More details about the Lippert-Magata calculations……3

Supporting Information Figure S1. Photophysical properties of **4**……4

Supporting Information Table S1. Compiled spectroscopic data for **4**……5

Supporting Information Figure S2. Dyad **4** fluorescence concentration plots……6

Supporting Information Figure S3. TGA and DSC curves for **4**……7

Supporting Information Figure S4. PXRD patterns for melted **4**……8

More details about the electronic properties of dyad **4**……9

Supporting Information Figure S5. Calculated frontier molecular orbitals for **4**……10

References……11

More details about the solution- and solid-state photophysical properties of 4

A broad absorption band was present for each solvent and the absorption maximum bathochromically shifted with increasing solvent polarity (Figure S1a). This shift changed from 403 to 419 nm from *n*-hexane to acetone. Interestingly, the absorbance band in DCM was the most bathochromically shifted (see Table s1). The width of the peak as well as its solvatochromicity (or increase in Stokes shift upon increasing solvent polarity) is suggestive of an intramolecular charge-transfer (ICT) band. Given the absorption data, we assume that the geometry of the MAN aromatic core relative to the NI core has only a minor effect on the solution-state photophysical properties of these dyads. Table S1 lists all the relevant spectroscopic data for dyad **4**.

A strong bathochromic shift in emission was observed upon dissolving **4** in solvents of varying polarity (Figure S1b). The dyad exhibits decreasing emission intensity upon going from *n*-hexane (ε 1.89) to acetone (ε 20.7) (because the fluorescence intensity was normalized this is not visible in Figure S1). The positive solvatochromism of the emission can be seen by the naked eye with **4** exhibiting a blue fluorescence in *n*-hexane, but a yellow/orange fluorescence in acetone. In particular, emission spectra of **4** in various solvents revealed a bathochromic shift of 135 nm upon going from *n*-hexane (λ_{max}, 444 nm) to acetone (λ_{max}, 579 nm). The large Stokes shift observed upon increasing the solvent polarity suggests that 1) polar solvents substantially stabilize the excited state of **4**, and 2) the absolute value of the excited state dipole moment is higher than that in the ground state.[1-2]

Concentration dependent emission fluorescence measurements were performed in order to verify the mode of electron transfer in the dyad excited state. Plotting the concentration versus emission intensity gave a linear relationship (Figure S2) indicating minimal concentration-dependent dyad fluorescence. This result, combined with the observed solvent-dependence of both the absorbance and emission, is strongly suggestive of an intramolecular photoinduced-electon transfer (PET) process rather than a Förster resonance energy transfer (FRET) process.

As previously stated, **4** gave two differently colored solids upon relatively faster (**4f**, yellow) and slower (**4s**, orange) evaporation from solvent. The solid-state absorbance and emission spectra for **4** are shown in Figure S2. **4f** shows a sharp absorbance peak at 398 nm while **4s** shows a peak at 542 nm with a smaller shoulder peak at 480 nm (Figure S2c). **4f** shows a strong emission at 545 nm while **4s** shows an emission peak at 576 nm (Figure S2d). Compared to the solution-state optical spectroscopy, the solid-state emission of **4f** and **4s** occur roughly where the emissions for the dyads in DCM (551 nm) and acetone (579 nm) occur, respectively.

More details about the Lippert-Magata calculations

In order to evaluate the excited state dipole moment of **4** a Lippert-Mataga plot was generated. The Lippert-Mataga plot evaluates the relationship between the solvent polarity parameter (Δ*f*) and the Stokes shift of the absorption and emission maxima ($\Delta\bar{\nu}$) using the Lippert-Mataga equation:

$$\bar{\nu}_A - \bar{\nu}_F = \Delta\bar{\nu} = \frac{2(\Delta\mu)^2}{hca^3}\Delta f + \text{constant}$$

where

$$\Delta f = \frac{\varepsilon - 1}{2\varepsilon + 1} + \frac{n^2 - 1}{2n^2 + 1}$$

and

$$a = \frac{3M}{4N\pi d}$$

where $\bar{\nu}_A$ and $\bar{\nu}_F$ are the absorption and fluorescence maxima in wave numbers (cm^{-1}), Δμ is the change in dipole moment ($\mu_{excited} - \mu_{ground}$), h is Plank's constant, c is the velocity of light in a vacuum, a is the Onsager cavity radius, ε and n are the dielectric constant of refractive index of a solvent, respectively, M is the molecular weight of the molecule, N is Avogadro's number, and d is the density of the molecule.[3-4] Our calculations assume the density of our dyad is 1. For the results shown below the polarity function of the solvents were calculated using the Lippert solvent polarity function.

The calculated Onsager radius for **4** was 10.922 Å. The ground state dipole moment (μgD) were calculated using the DFT method at the B3LYP G-31* level and was found to be 7.52 D. Using the Lippert-Mataga relationship, the excited state dipole moment (μeD) for **4** was calculated to be 54.99 D which amounts to an overall dipole change of 47.47 D upon going from the ground to excited state. These calculations confirm that the excited state of **4** has a significantly larger dipole moment, consistent with the observed solvatochromatic behavior and our DFT calculations. Quantum fluorescence yields (Φf) were calculated using the comparative method. Standards of 20, 15, 10, 5, and 2.5 μM concentrations were subjected to UV-Vis and fluorescence spectroscopy. Perylene in a solution of cyclohexane (Φf = 0.94) was used as standard due to its similar excitation range (360-420 nm).[5] For **4** a general decrease in fluorescence quantum yield upon increasing the polarity of the solvent was observed going from 0.31-0.04 (see Table 1). Other studies using 4-donor substituted 1,8-naphthalimide derivatives[6-8] and other dyes[9-10] exhibit the same decrease in fluorescence quantum yield as a result of increasing solvent polarity.

Supporting Information Figure S1. Photophysical properties of **4**. (a) Normalized solution-state absorbance spectrum; (b) Normalized solution-state fluorescence spectrum; (c) Normalized solid-state absorbance spectrum; (d) Normalized solid-state fluorescence spectrum.

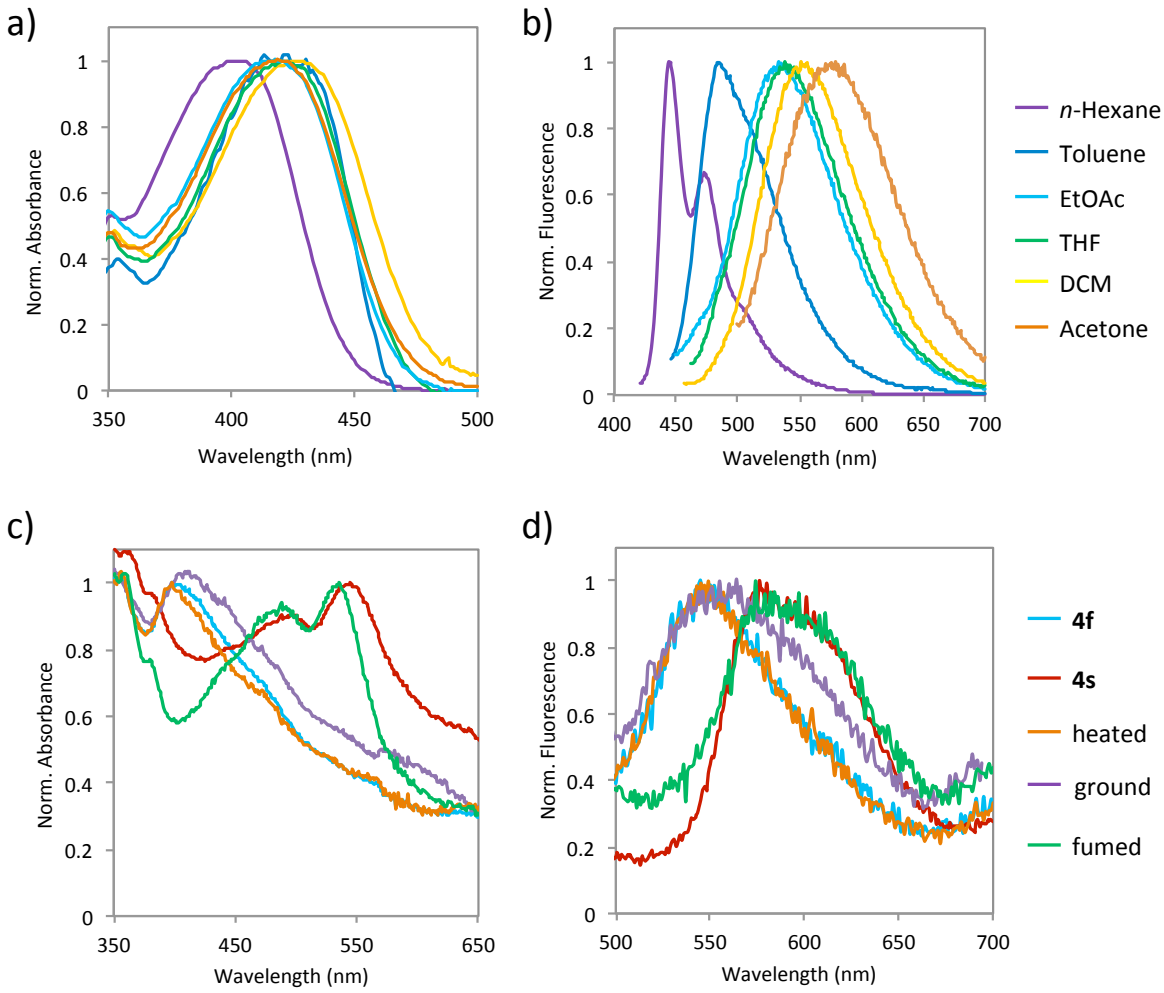

Supporting Information Table S1. Compiled spectroscopic data for **4**.

Solvent	λ_{max} Abs (nm)	λ_{max} Em (nm)	Fluorescence Quantum Yield (Φ_f)*	μ_g (D)**	μ_e (D)***
n-Hexane	403	444	0.31	7.52	54.99
Toluene	422	484	0.22		
Ethyl Acetate	418	538	0.17		
THF	421	533	0.16		
DCM	426	551	0.15		
Acetone	419	579	0.04		
Fast Evaporation **4f** (solid)	398	545	-		
Slow Evaporation **4s** (solid)	542	576	-		
After heating (solid)	398	549	-		
After grinding (solid)	404	546	-		
After vapor-fuming (solid)	536	574	-		

*All absorbances were kept below 0.1 at maximum excitation wavelength. Solid-state fluorescence quantum yields were not determined.

**Calculated using the DFT method in Spartan 08 at the B3LYP G-31* level. Ground dipoles for the planar geometries are shown.

***Calculated and extracted using the Lippert-Mataga relationship.

Supporting Information Figure S2. Dyad **4** fluorescence concentration plots showing a linear relationship between the concentration and the fluorescence intensity.

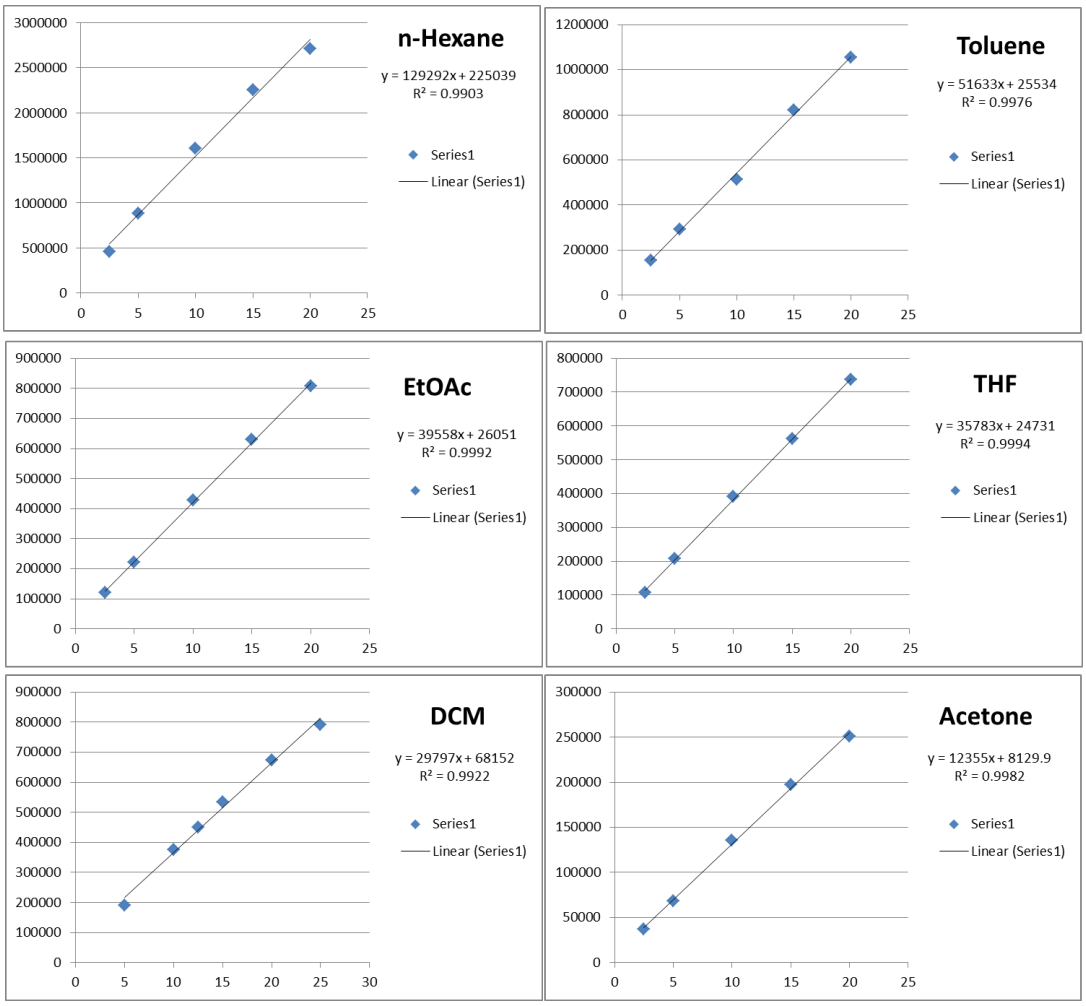

Supporting Information Figure S3. Images of the heat induced transformation of **4s** to **4f** by heating the single crystal at 110 °C for <1 minute (top) and the vapor-fuming induced transformation of **4f** to **4s** using DCM over the course of 24 hours (bottom).

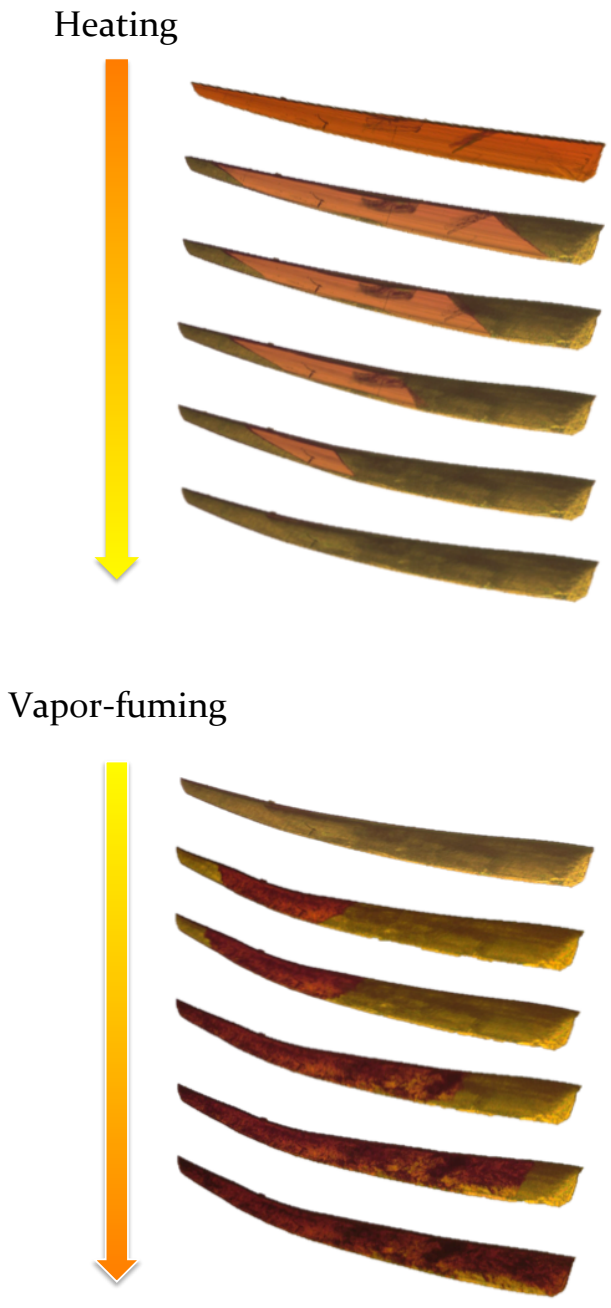

Supporting Information Figure S4. TGA (blue line) and DSC (red line) curves for **4** with both analyses heating at the same rate (5 °C per minute). The total sample weight for TGA was 7.5120 mg and the % weight loss as a function of temperature (90-110, 110-130 and 130-150 °C) is indicated with the double-sided arrows.

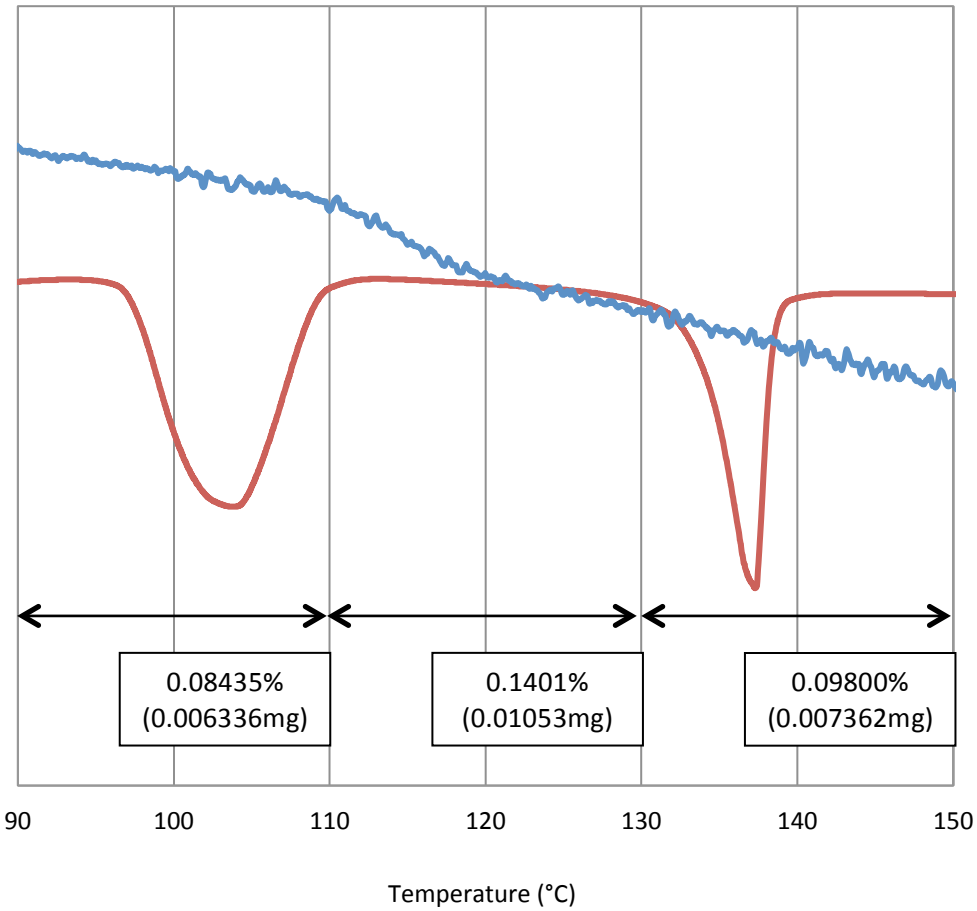

Supporting Information Figure S5. PWXRD patterns of two polymorphs of **4** after multiple forms of stimuli have been applied. The grey line shows that the morphology of **4** after having been melted and cooled to room temperature is the same as **4f**.

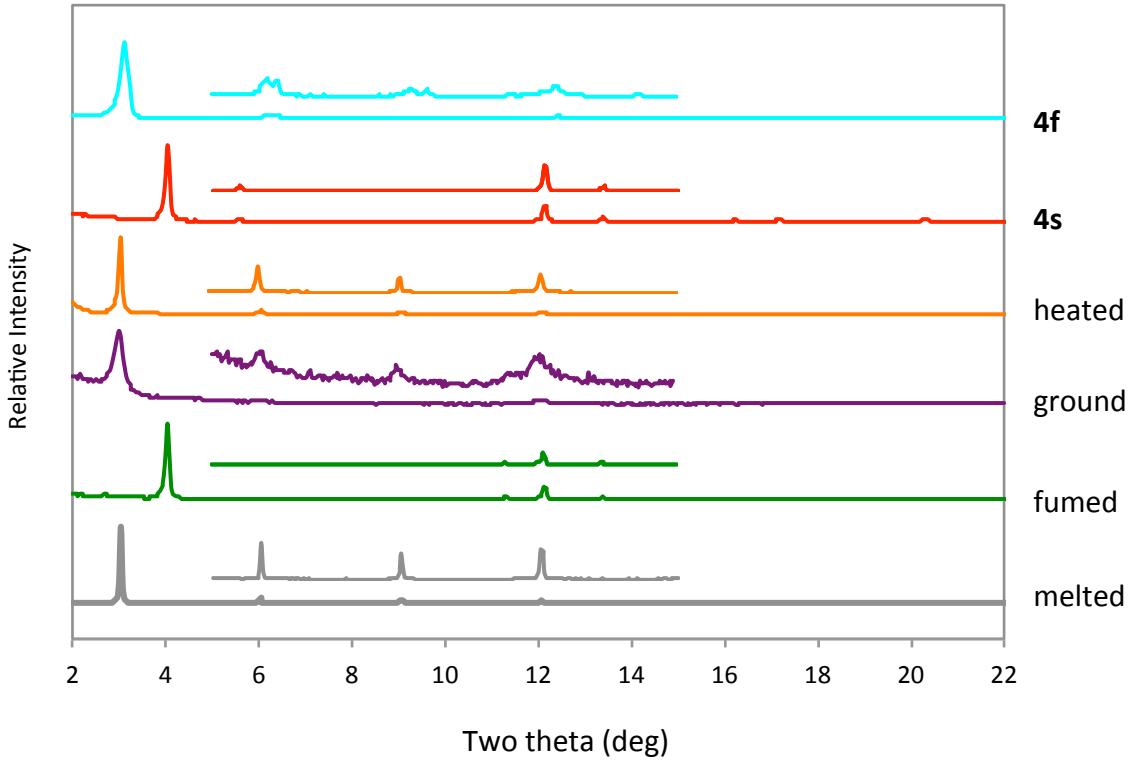

More details about the electronic properties of dyad 4

To get a better understanding of the electronic nature of these dyads, the frontier molecular orbital energy levels for **4** were calculated using the DFT method at the B3LYP G-31* level. Two geometries were used: a planar geometry, in which the rotation angle between the donor and acceptor moieties is 0° (as observed in the crystal structures for **4s**, **1f** and **1s**), and a twisted geometry, in which the donor and acceptor moieties are angled 90° to each other (Figure S6). The calculated HOMO and LUMO energy levels are listed in Figure S6 below. As shown below, the HOMO of **4** in both geometries resides primarily on the relatively more electron-rich MAN while the LUMO is located primarily on the relatively electron-deficient NI. In the planar conformations, both the HOMO and LUMO are slightly delocalized across the alkyne linker while the twisted conformation shows no delocalization of the HOMO and LUMO. This effect is common in frontier molecular orbital calculations of planar verses twisted aromatic molecules.[3,12-13] The physical separation between the HOMO and LUMO is consistent with internal charge-transfer (ICT).[2,4,9] The relative similarities between the HOMO and LUMO energy levels of **4** indicate that the geometry of the MAN aromatic unit relative to the NI aromatic unit likely plays only a small role in the electronic configuration of the dyads.

Supporting Information Figure S6. Calculated frontier molecular orbitals for **4** in planar and twisted geometries using the DFT method in Spartan 08 at the B3LYP G-31* level.

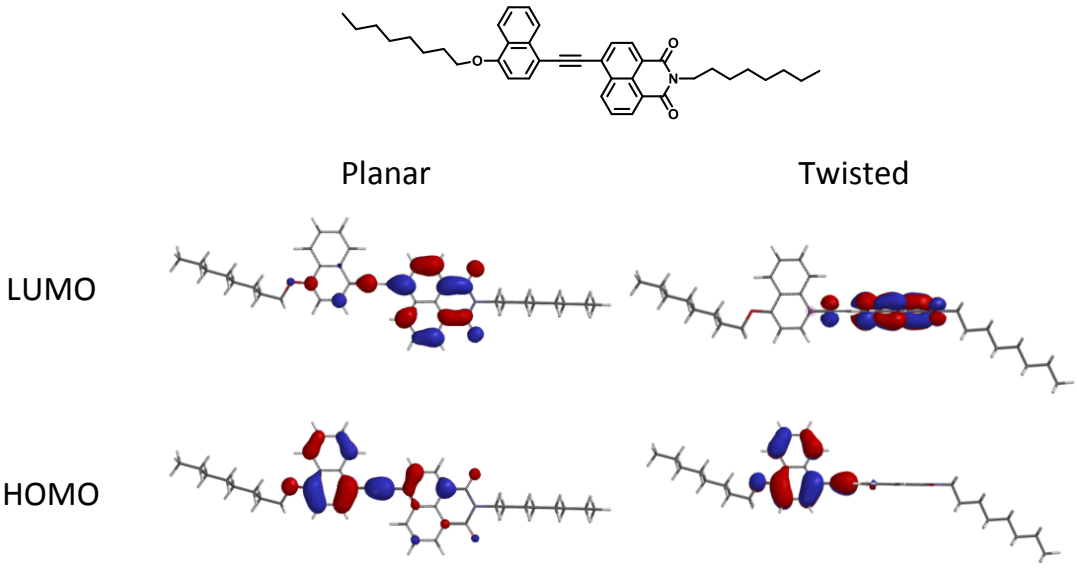

Alkyne Geometry	HOMO*	LUMO*	Gap*
Planar	-5.463	-2.484	2.979
Twisted	-5.581	-2.466	3.115

* Calculated using the DFT method in Spartan 08 at the B3LYP G-31* level. Energy in eV.

References

(1) Jiang, W.; Tang, J.; Qi, Q.; Wu, W.; Sun, Y.; Fu, D. *Dyes Pigments* **2009**, *80*, 11.

(2) Wang, L.; Zheng, Z.; Yu, Z.; Zheng, J.; Fang, M.; Wu, J.; Tian, Y.; Zhou, H. J. *J. Mater. Chem. C* **2013**, *1*, 6952.

(3) Chen, K.-F.; Chang, C.-W.; Lin, J.-L.; Hsu, Y.-C.; Yeh, M.-C. P.; Hsu, C.-P.; Sun, S.-S. *Chem. Eur. J.* **2010**, *16*, 12873.

(4) Raikar, U. S.; Tangod, V. B.; Mannopantar, S. R.; Mastiholi, B. M. *Optics Commun.* **2010**, *283*, 4289.

(5) Brouwer, A. *Pure Appl. Chem.* **2011**, *83*, 2213.

(6) Bag, S. S.; Pradhan, M. K.; Kundu, R.; Jana, S. *Bioorg. Med. Chem. Lett.* **2013**, *23*, 96.

(7) Saha, S.; Samanta, A. *J. Phys. Chem A* **2002**, *106*, 4763.

(8) Ma, J.; Zhao, J.; Yang, P.; Huang, D.; Zhang, C.; Li, Q. *Chem. Commun.* **2012**, *48*, 9720.

(9) Rao, S. M.; Liao, C.-W.; Su, W.-L.; Sun, S.-S. *J. Mater. Chem. C* **2013**, *1*, 5491.

(10) Grabowski, Z. R.; Rotkiewicz, K.; Rettig, W. *Chem. Rev.* **2003**, *103*, 3899.

(12) Sun, W.; Zhou, C.; Xu, C.-H.; Zhang, Y.-Q.; Li, Z.-X.; Fang, C.-J.; Sun, L.-D.; Yan, C.-H. *J. Phys. Chem. A* **2009**, *113*, 8635.

(13) Chen, R.; Zhao, G.; Yang, X.; Jiang, X.; Liu, J.; Tian, H.; Gao, Y.; Liu, X.; Han, K.; Sun, M.; Sun, L. J. *J. Mol. Struct.* **2008**, *876*, 102.